EXPERIMENTS IN MODERN PHYSICS
by MELISSINOS
P. 226-252

6

SCATTERING EXPERIMENTS

1. Introduction

Ever since Rutherford performed his original experiments on the scattering of energetic alpha particles from atomic nuclei, scattering has become increasingly more powerful as a tool for investigating the forces between elementary particles. By now it is familiar to the reader that an electron, under the influence of the attractive electromagnetic force of the nucleus, may be found in a bound state. The classical analogue of this situation is the motion of the planets around the sun under the influence of the gravitational force; they describe elliptical orbits.

According to Newton's laws, in the absence of a force, electrons (atoms, planets) will travel in a straight line,† since $(d\mathbf{p}/dt) = 0$. If, however, the trajectory of the electron passes by a nucleus, under the influence of the electromagnetic force, two things may happen: either the electron will fall into a bound state, or, if its total energy is larger than the ionization potential, its trajectory will be altered but it will not become bound to the

† A remarkable experimental confirmation of this statement is obtained in atomic-beam experiments.

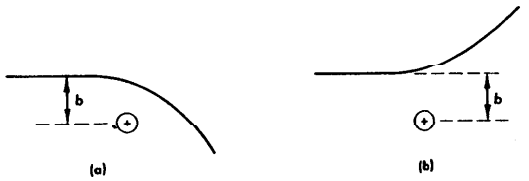

FIG. 6.1 Scattering of a particle due to the presence of a force center. (a) Attractive force. (b) Repulsive force.

nucleus. The latter is shown in Fig. 6.1 and we speak of "scattering" of the electron by the nucleus. The classical analogue of this situation is the motion of "comets" under the influence of the gravitational force; they describe hyperbolic orbits.

Scattering is electromagnetic in the electron-nucleus system, and gravitational in the comet-sun system. In general by investigating scattering processes we may obtain information on the nature and strength of any force that may exist between projectile and target. In particular, we already know the form of both the gravitational and electromagnetic force

$$F_e = k\frac{e_1e_2}{r^2} \qquad F_g = G\frac{m_1m_2}{r^2} \tag{1.1}$$

Here k, and G are constants, e_1e_2 and m_1m_2 are the electric charges or gravitational masses, and r the distance between projectile and target. From Eq. 1.1, we see that the shorter the distance, the stronger the force. Strong forces lead to *large-angle scattering*, which therefore must be a consequence of a close approach of the projectile to the target. The distance of closest approach is related to the *impact parameter* b, which is the distance from the target normal to the extension of the undeflected trajectory of the projectile as shown in Fig. 6.1.

Equation 1.1 is correct under the condition that the charges (masses) are concentrated at one point, or at least that the smallest distance r is always much larger than the extent over which the charge is distributed; if this is not true, the force will be given by an appropriate extension of Eq. 1.1

$$F = ke_1\int \frac{\rho(r')}{|\mathbf{r} - \mathbf{r}'|^2}\,d\mathbf{r}' \tag{1.2}$$

where $\rho(r')$ is now the charge density of the target and we have assumed that the projectile is a point charge. Thus, if the force law is known, scatterings with small impact parameters may provide information on the struc-

ture of the target. As a matter of fact, the process of human vision consists of the detection by the eye of quanta of electromagnetic radiation, scattered by the objects that are seen. In this process, however, the distance of closest approach is very much smaller than the dimensions of the object and, consequently, the resolution is good. Radar detection is similar, the only difference being that the wavelength of the radiation is longer and consequently the resolution is poorer.

Since the scattered particle moves in the field of force of the target, work is done, with consequent changes in potential and kinetic energy. However, when the projectile and target are considered together as a system (isolated), there can be no change in its total energy: what takes place is a transfer of energy and momentum from the projectile to target; if the projectile is scattered by an angle θ, the momentum transfer is

$$q = |\mathbf{p}_i - \mathbf{p}_f| = \sqrt{p_i^2 + p_f^2 - 2p_i p_f \cos\theta} \tag{1.3}$$

and if the energy of the projectile is not much altered in the scattering process, $|p_i| = |p_f|$

$$q = 2p \sin\frac{\theta}{2} \tag{1.4}$$

The momentum transfer is the basic physical quantity that characterizes all scattering experiments; it depends on the momentum (rigidity) of the projectile and the angle of scattering. The probability for scattering is, to first order, a function only of the momentum transfer (and not of the angle), large momentum transfer scatters being, in general, less probable.

In the process of scattering, if the target is very massive, as compared to the momentum transferred, it is clear that the energy transferred to it, ΔE, will be small, since

$$\Delta E = T = \sqrt{m^2 + q^2} - m \simeq \frac{1}{2}\frac{q^2}{m} \tag{1.5}$$

In Eq. 1.5 we assumed that all the transferred energy appeared as kinetic energy of the target; in this case we speak of *elastic* scattering. However, it is possible that in the scattering process the target may be excited to a state of different energy (we may write this as $m_f \neq m_i$), or that part of the transferred energy is converted to mass in the form of new particles, or that the target dissociates itself with the absorption or liberation of energy; in these cases we speak of *inelastic* scattering.

Besides gravitational and electromagnetic forces, today we know of two other types of force fields: the *nuclear force* (or *strong interaction force*) and the *weak interaction force*. The former is responsible for holding nuclei together, and the latter is responsible for the radioactive decay of nuclei with the emission of an electron (or positron). In Table 6.1 are given the relative strengths of the four force fields presently known to man.

TABLE 6.1
THE FOUR FORCE FIELDS AND THEIR RELATIVE STRENGTH

Force field	Strength	Main manifestation
Nuclear force	1.0	Binding of nuclei
Electromagnetic forces	1/137	Binding of atoms, molecules; also macroscopic effects
Weak interaction	10^{-14}	Decay of elementary particles
Gravitational force	10^{-42}	Everyday experience

In scattering between elementary particles, the probability for scattering (cross section) is related to the strength of the interaction as given in Table 6.1. Therefore, strong-interaction scattering (as of a neutron from a proton) is easier to observe than electromagnetic scattering (as of an electron from a proton) at the same momentum transfer. Weak interaction scattering has a much smaller cross section and was only recently (1962) observed in the inelastic scattering of neutrinos, $\nu_\mu + n \rightarrow \mu^- + p$. Gravitational scattering, while absurdly small at the elementary particle level, is, however, observed macroscopically.

The three scattering experiments described in this chapter are all due to the electromagnetic interaction. In the first experiment, alpha particles (nuclei of helium) of sufficient energy (5.2 MeV) are scattered from the nucleus of gold by virtue of the interaction of the alpha-particle charge, $Z = +2$, with the charge of the gold nucleus $Z = 79$. It is true that a nuclear-force interaction also exists between these two particles. Even though the nuclear force is stronger, its range is short, so that unless the alpha particles have sufficient energy to overcome the repulsive Coulomb potential, they cannot approach close enough to the nucleus to be affected by the nuclear force. If we take for the range of the nuclear force 10^{-13} cm, the Coulomb potential will be

$$\Phi \simeq \frac{e^2}{4\pi\epsilon_0}\frac{Z(\text{He})Z(\text{Au})}{10^{-13}}\ (\text{MKS units}) = 230\ \text{MeV}\dagger$$

which a 5.2-MeV alpha particle can clearly not overcome (see Fig. 6.2).

† $230\ \text{MeV} = \frac{(1.6 \times 10^{-19})^2}{1.0 \times 10^{-13}} \times 9 \times 10^9 \times \frac{2 \times 79}{10^{-13}}$ eV

Such alpha-particle scattering experiments were first performed by E. Rutherford in 1910 and are named after him.

In the second experiment, photons of an energy of 662 keV are scattered from atomic electrons. At these energies, the momentum transfer is large enough so that the electrons may be considered free and, consequently, the energy transfer also becomes considerable; therefore, the energy of the scattered photon is decreased as a function of the angle of scattering. As a result, a continuous shift is observed in the frequency of the scattered radiation, a result inexplainable on the basis of a classical theory of radiation. The first experiments of this type were performed with x-rays by A. H. Compton in 1923 and are now named after him. The simple assumption that the scattering of the flux of electromagnetic radiation can be described by the scattering of individual quanta carrying energy and momentum leads to the correct explanation of the effect. It is the electromagnetic interaction, but now taking place between the photons and charged particles, that is responsible for the scattering.

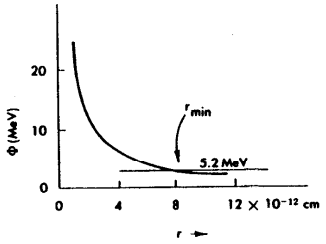

FIG. 6.2 The coulomb (electrostatic) potential of a gold nucleus as a function of the distance from it; r_{min} is the closest distance that a 5.2 MeV alpha particle can reach.

The third experiment described concerns again the electromagnetic interaction of photons with an electric charge, now the charge of the nucleus. However, the scattering is completely inelastic, resulting in the absorption of the photon by the nucleus; to satisfy energy and momentum conservation, and in order for this absorption process to take place, the photons must have exactly the correct energy: we speak of resonant absorption of gamma rays. This effect was first observed by R. Mössbauer (1960) and is now named after him; since the very narrow band of gamma-ray energies over which the absorption takes place is of the order of 1 part in 10^{12}, the Mössbauer effect is the most precise measurement of frequency (or for that matter, the most precise measurement of any kind) that man has ever performed.

2. Rutherford Scattering

2.1 Derivation of the Scattering Cross Section

We shall now derive the *differential cross section* $d\sigma/d\Omega(\theta, \varphi)$, for an alpha particle scattered by the Coulomb field of the nucleus into the element of solid angle $d\Omega$ centered about the angles θ and φ. To do this we will first find an expression for the angle of the scattered particle as a function of the impact parameter b.

Consider therefore Fig. 6.3a, where the initial position and velocity of the alpha particle is $\mathbf{v}_i$, and the impact parameter b. Since the force is always directed along the line joining the projectile and target, the motion will be in the plane defined by $\mathbf{v}_i$ and the position of the scattering center. We will first obtain the equation for the orbit†. The equations of motion can be had either through Lagrangian formalism, or from Newton's equations (CGS units are used)

$$m\ddot{r} - mr\dot{\theta}^2 = \frac{ee'}{r^2} \tag{2.1}$$

$$\frac{d}{dt}(mr^2\dot{\theta}) = 0 \tag{2.2}$$

Here the notation of Fig. 6.3a has been used and e and e' are the charges of target and projectile, respectively.

We can immediately obtain a "first integral" of Eq. 2.2, namely,

$$mr^2\dot{\theta} = \text{constant} = l \tag{2.3}$$

where l, the angular momentum about the scattering center, is conserved for all central force fields. Using Eq. 2.3 in Eq. 2.1 we obtain

$$m\ddot{r} - \frac{l^2}{mr^3} - \frac{ee'}{r^2} = 0$$

or

$$m\ddot{r} = -\frac{\partial}{\partial r}\left[\frac{l^2}{2mr^2} + \frac{ee'}{r}\right] \tag{2.4}$$

and multiplying by $\dot{r}$ both sides of Eq. 2.4

$$m\ddot{r}\dot{r} = \frac{m}{2}\frac{d}{dt}(\dot{r}^2) = -\frac{dr}{dt}\frac{dg}{dr} = -\frac{dg}{dt} \tag{2.5}$$

† For a detailed treatment of the two-body central force problem, see H. Goldstein, *Classical Mechanics*, Addison-Wesley, Chapter III.

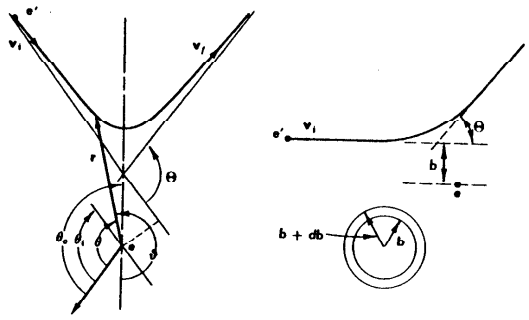

(a) (b)

FIG. 6.3 The scattering of a particle of charge e' from a particle of charge e; $\mathbf{v}_i$ and $\mathbf{v}_f$ are the initial and final velocities. The scattering angle is Θ. (a) Definition of the angles appearing in the derivation of the cross section. (b) The range of impact parameters b in db that contribute to scattering at Θ into $d\Omega$.

with

$$g = \frac{l^2}{2mr^2} + \frac{ee'}{r}$$

Integration of Eq. 2.5 yields

$$\frac{1}{2}m\dot{r}^2 + \frac{1}{2}\frac{l^2}{mr^2} + \frac{ee'}{r} = \text{constant} = E \tag{2.6}$$

The second "first integral" is the total energy of the alpha particle, which is conserved since the scattering is assumed to be elastic (we also assumed that the scattering center at the origin does not move). Note that Eq. 2.6 reduces correctly to $E = \frac{1}{2}mv^2$ for $r \to \infty$. Solving Eq. 2.2 and Eq. 2.6, we have

$$\frac{d\theta}{dt} = \frac{l}{mr^2} \tag{2.6a}$$

and

$$\frac{dr}{dt} = \sqrt{\frac{2}{m}\left[E - \frac{l^2}{2mr^2} - \frac{ee'}{r}\right]} \tag{2.6b}$$

Equations 2.6a and 2.6b may be combined to give the differential equation of the orbit

$$\frac{d\theta}{dr} = \frac{l}{m}\frac{1/r^2}{\sqrt{(2/m)[E - (l^2/2mr^2) - (ee'/r)]}} \tag{2.7}$$

In order to integrate Eq. 2.7, we make the change of variable

$$u = \frac{1}{r} \qquad du = \frac{-dr}{r^2}$$

so that

$$d\theta = \frac{-du}{\sqrt{-u^2 - (2ee'm/l^2)u + (2Em/l^2)}} \tag{2.8}$$

hence

$$\theta = \arccos\left[\frac{(l^2/ee'm)u + 1}{\sqrt{(2El^2/(ee')^2m) + 1}}\right] \tag{2.9}$$

and finally the equation of the orbit is

$$u = \frac{1}{r} = \frac{ee'm}{l^2}[\epsilon\cos(\theta - \theta_0) - 1] \tag{2.10}$$

where

$$\epsilon = \sqrt{\frac{2El^2}{(ee')^2m} + 1} > 1, \qquad \text{since } E > 0 \tag{2.11}$$

θ_0 is a constant of integration, such that at θ_i, $\cos(\theta - \theta_0) = 1/\epsilon$, as shown in Fig. 6.3a. If instead we choose to express the angles in terms of ϑ, we have

$$\cos(\theta - \theta_0) = \cos(\pi - \vartheta) = -\cos\vartheta$$

and

$$\frac{1}{r} = -\frac{ee'm}{l^2}(1 + \epsilon\cos\vartheta) \tag{2.12}$$

which is the equation of a hyperbola, with the focus at the origin, eccentricity ϵ, and center at $\vartheta_0 = \pi$, $r_0 = l^2/[ee'm(\epsilon - 1)]$. The limits on the angle ϑ are from

$$\cos\vartheta_1 = -\frac{1}{\epsilon} \qquad \frac{3\pi}{2} < \vartheta < \pi$$

to

$$\cos\vartheta_2 = -\frac{1}{\epsilon} \qquad \pi < \vartheta < \frac{\pi}{2} \tag{2.13}$$

The angle Θ through which the alpha particle was scattered is given by

$$\Theta = \pi - (\vartheta_1 - \vartheta_2) = 2\left(\frac{\pi}{2} - \cos^{-1}\frac{1}{\epsilon}\right) = 2\sin^{-1}\frac{1}{\epsilon}$$

$$\sin\frac{\Theta}{2} = \frac{ee'}{\sqrt{(2E/m)^2 b^2 + (ee')^2}} \tag{2.14}$$

It is convenient to use in Eq. 2.14 the impact parameter b; we have

$$b = (mv_i b)^2$$

and since

$$E = \tfrac{1}{2}mv_i^2$$

$$\sin\frac{\Theta}{2} = \frac{1}{\sqrt{(2Eb/ee')^2 + 1}} \tag{2.15}$$

$$\cot\frac{\Theta}{2} = b\frac{2E}{ee'}$$

Next we wish to obtain the probability for scattering through an angle Θ, at the azimuth φ; from Eq. 2.15 we see that there is no dependence on φ and the angle of scattering Θ is uniquely determined by the impact parameter b. To obtain the differential cross section for scattering into an angle (as defined in Chapter 5, Section 2) we note that the probability of the incident particle having impact parameter b in db is proportional to the element of area that can contribute to b. From Fig. 6.3b this is evidently

$$P(b)\,db = 2\pi b\,db$$

And the probability that a particle with b in db is scattered by the angle Θ in $d\Theta$ is

$$P(\Theta)\,d\Theta = P(b)\left(\frac{db}{d\Theta}\right)d\Theta = (2\pi b)\left(\frac{db}{d\Theta}\right)d\Theta$$

Substituting expressions for b and $db/d\Theta$ obtained from Eq. 2.15,

$$db = -\frac{ee'}{4E}\frac{1}{\sin^2\Theta/2}\,d\Theta$$

we have

$$dP(\Theta) = \frac{1}{8}\left(\frac{ee'}{E}\right)^2\frac{2\pi\cos\Theta/2}{\sin^3\Theta/2}\,d\Theta$$

$$dP(\Theta) = \left(\frac{ee'}{4E}\right)^2\frac{1}{\sin^4\Theta/2}\,2\pi\sin\Theta\,d\Theta \tag{2.16}$$

Since the scattering into φ is isotropic

$$\int_0^{2\pi} d\varphi = 2\pi$$

and we may write

$$d\sigma(\Theta, \varphi) = \frac{P(\Theta)\,d\Theta\,d\phi}{2\pi} = \left(\frac{ee'}{4E}\right)^2\frac{1}{\sin^4\Theta/2}\sin\Theta\,d\Theta\,d\varphi$$

And since the element of solid angle is $d\Omega = \sin\Theta\,d\Theta\,d\varphi$,

$$\frac{d\sigma}{d\Omega} = \left(\frac{ee'}{2}\right)^2\frac{1}{4E^2}\frac{1}{\sin^4\Theta/2} \tag{2.17}$$

which is the famous Rutherford scattering cross section.

Since our derivation was nonrelativistic, we may write $E = p^2/2m$, in which case

$$\frac{d\sigma}{d\Omega} = (2mZZ'e^2)^2\frac{1}{q^4} \tag{2.18}$$

where we used Ze and $Z'e$ for the charge of scatterer and projectile and $q = 2p\sin\Theta/2$ for the momentum transfer as defined by Eq. 1.4. Equation 2.18 shows clearly that the scattering cross section is a function of q *only* and in this case a very simple one.

A typical feature of Eq. 2.17 is that it increases very rapidly for small angles and even becomes infinite at $\Theta \to 0$; the relevant point is that even the total cross section

$$2\pi\left(\frac{ZZ'e^2}{4E}\right)^2\int_{\Theta_0}^{\pi}\frac{\sin\Theta}{\sin^4\Theta/2}\,d\Theta = (ZZ'e^2)^2\frac{\pi}{2}\left[\frac{1}{\sin^2\Theta_0/2} - 1\right]_{\Theta_0\to 0}^{\to\infty} \tag{2.19}$$

goes to infinity if scattering through small angles is included. This fact is a reflection of the long-range nature of the electromagnetic force†; small-angle scattering corresponds to very large impact parameters. It is this property of electromagnetic scattering that gave rise to "multiple scattering" as discussed in the Chapter 5. It is easy, however, to see that a cutoff in the smallest possible scattering angle Θ_0 (Eq. 2.19) must be imposed from physical considerations. That is, the largest permissible impact parameter b_0 is determined by the transverse size of the beam, or of the scatterer (whichever one is the largest). But even long before that limit is reached, the impact parameter cannot be larger than the size of the atom, since outside it the charge of the nucleus is "screened" by the atomic electrons.

† As compared to the nuclear force.

It is interesting that even though Eq. 2.17 was derived on classical arguments, it is also correct quantum mechanically. The same result is obtained by an exact solution of the Schrödinger equation for a Coulomb potential†, as well as by a first-order perturbation theory (Born approximation) treatment. We remark also that the same scattering cross section is obtained when the potential is attractive, the two cases being experimentally indistinguishable (as shown in Fig. 6.1). We know, however, that for the electromagnetic force the potential is "attractive" for particles of opposite charge and "repulsive" for particles of the same charge.

2.2 Scattering of Alpha Particles by the Nucleus of Gold

We will now describe in detail a measurement of the scattering of polonium 210 alpha particles from a very thin foil of gold. The apparatus used is, in essence, similar to that of Rutherford's except for the detection technique. As in any scattering experiment we need:

(1) *The beam of particles to be scattered.* The alpha particles (He^4 nuclei) from Po^{210} decay are ideally suited for this purpose, since (a) they have sufficient energy (5.2 MeV) to traverse a thin target; (b) the beam is monoenergetic and does not contain electrons; (c) the high intensity of a radioactive source permits adequate collimation to yield a narrow beam; (d) they are readily available.‡

(2) *The target, or scattering material.* This needs to be sufficiently thick to produce enough scattering events for the available incident-beam intensity; but it should not be so thick as to change appreciably the energy of the primary beam or to affect the scattered alpha particles.§ The target thickness used is of the order of a few mg/cm².

(3) *The detector.* In this apparatus a thin piece of scintillating material (organic) mounted onto a photomultiplier was used.¶ Since the range of 5.2-MeV alphas in air is only approximately 4 cm, the beam, scatterer, and detector must all be enclosed in a vacuum. The detector can be moved to different angles with respect to the beam line, so that the angular distribution of the scattered alpha particles may be obtained.

The apparatus is shown in Fig. 6.4a; it consists of the cylindrical vessel A, containing the beam source, target holder, and detector; vessel A can

† See, for example, M. Born, *Atomic Physics*, Hafner Publishing Co., 1957. Appendix XX, p. 360.

‡ To accelerate an alpha particle to this energy one would need a potential difference of 2.6×10^6 eV (Van de Graaf generator) or would have to use a cyclotron.

§ It should not be thicker than a fraction of a mean free path.

¶ A solid-state counter (as described in Chapter 5, Section 5.2) may also be used to detect the alpha particles. It has the advantage of simplicity and better discrimination against background.

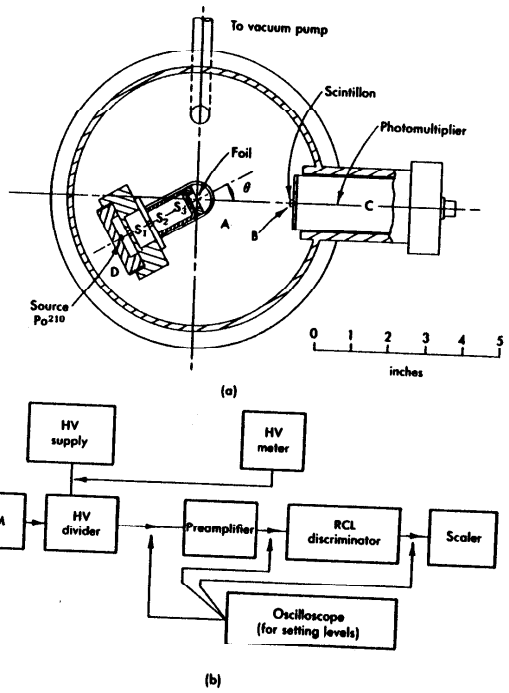

FIG. 6.4 Apparatus used for Rutherford scattering experiment. (a) The scattering chamber, source, target and detector. (b) Block diagram of the electronics.

be readily evacuated. The thin slab of scintillon† B, of width 0.565 cm, height 1.55 cm, and thickness 0.15 cm, is the detecting element, and is glued onto a 6192 DuMont photomultiplier tube C; the photomultiplier is permanently set into the scattering chamber with the vacuum seal made at its plastic base (one should ascertain that the tube does not get drawn

† The material used was Pilot B (Pilot Chemicals, Inc., 36 Pleasant St., Watertown, Mass.).

into the chamber when it is first pumped down). For the beam source, 0.5 millicuries of Po^{210} were plated on the inside of the round cap D, which can be unscrewed easily for removal. Three slits, S_1, S_2, and S_3, 1 mm by 1 cm, are used to collimate the flux of alpha particles emitted by the source. Beyond the third slit, the target holder can be positioned; it consists of a small 2 cm by 2 cm frame on which the scattering foil (gold, aluminum, etc.) is mounted.

Usually the detector is swung around the incident-beam direction. In the present setup, however, it is more convenient to have the detector fixed and to rotate the beam and scattering foil. This latter assembly is mounted as a whole on a shaft coaxial with the scattering center, and can be moved without breaking the vacuum; a pointer outside the chamber indicates the angle of rotation. The associated circuitry (Fig. 6.4b) is the standard one consisting of the high-voltage supply and divider for the photomultiplier, a preamplifier, and an RCL 20506 single-channel discriminator driving a scaler, as described in Chapter 5, Section 4.2.

The counts that register on the scaler do not all come from scattered alpha particles but contain "background" of two types:

(a) A counting rate R'', which is present even when the source is removed from the chamber. This is due mainly to contamination of the chamber with Po^{210}, and to noise in the detector or electronics. To measure R'' the source is removed and a count is taken at different angles; it is usually independent of angle.

(b) A counting rate R' due to the source, but not produced by scattering in the target material itself. The rate R' is mainly due to poor beam collimation, slit scattering, scattering off residual air molecules, and so on. To measure R', the source is placed in position, but the scattering foil is removed and again a count is taken at different angles. This time an angular dependent background may be expected.

Since R' contains R'',† the true rate is given by

$$R_{\text{true}}(\theta) = R(\theta) - R'(\theta) \tag{2.20}$$

where R is the counting rate with both source and target in place. It is necessary to know R' and R'' separately in order to understand the causes of the background and thus reduce it as much as possible.

Let us next make some quantitative estimates on the expected counting rates. The defining beam slit is 1 mm by 1 cm at a distance of 5 cm, and hence subtends a solid angle

$$\Delta\Omega(\text{beam}) = 4 \times 10^{-2}\ \text{sr}$$

† Unless the scattering foil is contaminated, which can be readily ascertained.

We thus obtain for the beam intensity

$$0.5 \times 10^{-2} \times 3.7 \times 10^{10} \times \frac{.004}{4\pi} = 6000\ \text{counts/sec}$$

The observed beam intensity, however, is 110,000 counts/min, the difference from our simple estimate being due in part to the extent of the source but mainly to self-absorption in the source.

Next we consider the detector solid angle. The size of the scintillon is 0.873 cm^2 at a distance of 6.66 cm, hence

$$\Delta\Omega \sim 0.02\ \text{sr}$$

If we use a gold foil of thickness 0.0001 in., and

$$Z' = 2; \quad Z = 79; \quad \text{and} \quad E = 5.2\ \text{MeV}$$

we obtain†

$$\frac{d\sigma}{d\Omega} = \left[\frac{2 \times 79}{4\pi\epsilon_0} \frac{(1.6 \times 10^{-19})^2}{5.2 \times 10^6 \times 1.6 \times 10^{-19}} \frac{1}{4}\right]^2 \frac{1}{\sin^4\theta/2} = \frac{1.20 \times 10^{-30}}{\sin^4\theta/2}\ \text{m}^2$$

Thus for scattering through 15°

$$\frac{d\sigma}{d\Omega}(\theta = 15°) = 4.17 \times 10^{-21}\ \text{cm}^2$$

The number of alphas scattered into the detector is given by

$$I_s = I_0 N \frac{d\sigma}{d\Omega} d\Omega$$

where

$I_0 = 1.1 \times 10^5$ counts/min in the incident beam

$d\Omega = 2 \times 10^{-2}$ sr

$N = t \times \rho \times (N_0/A)$, the area density of scatterers, where

$N_0 = 6 \times 10^{23}$, Avogadro's number

$\rho = 19.3$ gr/cm^3, the density of the scatterer (gold)

$t = 0.00025$ cm, the thickness of the foil

$A = 197$, the atomic weight of gold

† Note that we calculate in the MKS system and that dimensionally

$$[(Z'e^2)/(4\pi\epsilon_0)]^2 = [F]^2[L]^2 \quad \text{while} \quad E^2 = [F]^2[L]^2.$$

This yields

$$N = 1.48 \times 10^{19} \text{ gold nuclei/cm}^2$$

and

$$I_s(\theta = 15°) = 132 \text{ counts/min}\dagger$$

This seems to be a sizable rate; however, the pertinent question is how this rate compares to the background rate R', that is, what is the signal-to-noise ratio (S/N). In the present experiment, the background (mainly due to the contamination of the vessel) was high, and of the order of 130 counts/min; thus already at 15°, $S/N = 1$.

To improve the S/N ratio, we could increase I_s by increasing the solid angle (which is impractical), or by increasing the beam intensity (which might raise the noise level as well) or most simply, by increasing the scattering-foil thickness. If we increase the foil thickness, however, we are limited by the energy loss of the beam particles in the target. If we wish, for example, to determine the cross section to 25 percent, then since

$$\frac{d\sigma}{d\Omega} \propto E^{-2}$$

and

$$\frac{\Delta(d\sigma/d\Omega)}{d\sigma/d\Omega} = -2\frac{\Delta E}{E}$$

the energy loss must not exceed 12 percent. By referring to the Bragg curve (Fig. 5.42) we note that a 5.2-MeV alpha particle will lose 1.5 MeV of its energy after traversing the equivalent of 1.2 cm of air at stp, namely, approximately 2 mg/cm², which corresponds to a gold foil of thickness $t = 0.00012$ cm.‡

Multiple scattering in the foil is not significant for the alpha particles. We use Eq. 2.17, Chapter 5, and $L_{rad} \approx 6$ gr/cm² for gold; then with the above value $t = 0.00025$ cm, we obtain

$$\theta_{rms} = \frac{21.2}{\sqrt{2mE}} Z^2 \sqrt{\frac{10^{-3}}{0}} \text{ rad} \simeq 0.25°$$

† $I_s(\theta = 15°) = 1.1 \times 10^5 \times 1.5 \times 10^{19} \times 2 \times 10^{-3} \times 4 \times 10^{-21}$.

‡ From Chapter 5 we see that energy loss/(gm/cm²), $dE/d\xi = N_0(Z/A)z^2 f(I, \beta)$, yielding the equivalent thickness of gold $t = 0.00012$ cm. However, at these low velocities a more detailed treatment of the energy loss is required, and as also observed experimentally the alpha particle loses 1.5 MeV after traversing a gold foil of thickness $t = 0.00025$ cm (see also Fig. 5.4).

2.5 Results and Discussion

We now will give results for Rutherford scattering obtained by students† with the apparatus described in Section 2.2.

It is important to be extremely careful when handling the radioactive source for this experiment; polonium, while very convenient for Rutherford scattering, is a "nasty" isotope. As noted in Chapter 4, it can be lethal when taken internally, and due to the recoil following alpha emission, small parts of the source break off and contaminate the vessel in which it is enclosed. Further, alpha-particle contamination cannot be detected with a Geiger counter, but only with special alpha detectors, such as a gas-flow counter‡. *Gloves must always be worn* when handling the source, and the cap must be replaced whenever the source is removed from the apparatus.

First the chamber is evacuated and the detection system is adjusted with the source in place, but without the scattering foil. The detector is placed at 0° and the photomultiplier output is observed on an oscilloscope; the high voltage is then raised until clean pulses of a few volts amplitude are obtained. Next the discriminator is adjusted by taking a plateau curve in the integral mode; it is also possible to operate the discriminator in the differential mode, but in either case attention must be paid to the energy loss of the alphas when the foil is inserted.

We are now in a position to measure the beam profile when the scatterer is *not* in place; the results of counting rate against angle are shown on a linear scale in Fig. 6.5a and on a logarithmic scale in Fig. 6.5b. This measurement serves three purposes:

(a) It determines the background rate R' and gives the extent of the beam, namely, the detector angles beyond which the counts will be due to scattered alphas. From Fig. 6.5b we see that for $\theta \gtrsim 6°$ there are no beam counts; also the value of the background is 130 counts/min. (As noted earlier, this rate was due almost entirely to contamination of the chamber, as evidenced by a separate measurement with the source removed).

(b) It provides the information on the incoming beam intensity, and for this purpose the linear plot of Fig. 6.5a is more useful. If the over-all beam dimensions are smaller than the dimensions of the detector, then the peak count simply gives the beam intensity and the profile of Fig. 6.5a should have a flat top.

This is not always true, however. Let us first consider the distribution of the beam in the θ direction (horizontal); this may be uniform, or Gaussian, or of another type. Let the interval $\Delta\theta = x$ contain 90 percent of the beam

† R. Dockerty and S. McColl, class of 1962.

‡ PAC 3G Gas Proportional Counter; may be purchased from Eberlein Instruments Corp., Sante Fé, N. M.

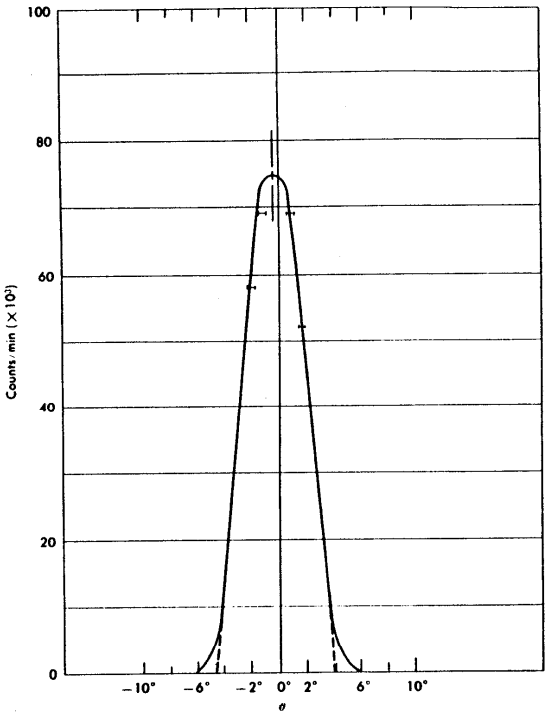

FIG. 6.5 The profile of the alpha particle beam as measured in the scattering chamber with the scattering foil removed. (a) (*Above*) Linear plot that is used for obtaining the total flux, and the beam center. (b) (*Opposite page*) Semilogarithmic plot giving the background level outside the beam.

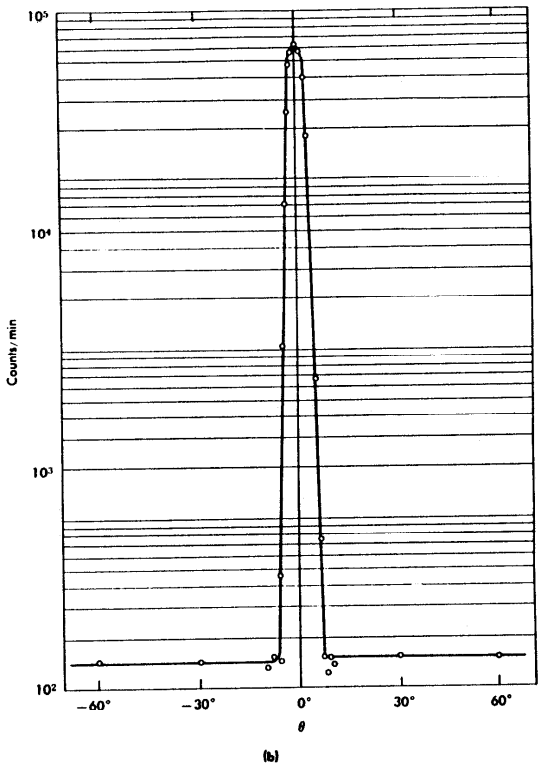

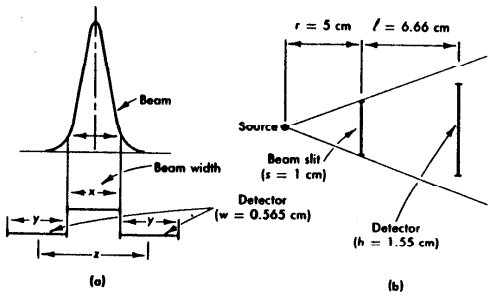

FIG. 6.6 The effects of the finite dimensions of the beam and of the detector. (a) In the horizontal plane. (b) In the vertical plane.

(see Fig. 6.6a). The angular width of the detector is

$$\Delta\theta = y = \frac{0.565}{6.66} \times \frac{180}{\pi} = 4.^{\circ}9$$

Further, from Fig. 6.5a we observe that the beam counts drop to 10 percent of their peak value in $\Delta\theta = z = 8.^{\circ}5$ (by extrapolating to zero beam count, we obtain $\Delta\theta = z' = 9°$). As seen in Fig. 6.6a, $z = x + y/2 + y/2$, so that we find $x \simeq 3.^{\circ}6$, which is smaller than the detector width; consequently we must expect in the profile of Fig. 6.5a a flat top of width $\Delta\theta = y - x \approx 1.^{\circ}3$.

Unfortunately in the vertical direction, the beam size is larger than the dimension of the detector, as is seen in Fig. 6.6b, where the dimensions of the beam-defining slit and the detector are shown. We note that only a fraction F of the incident beam reaches the detector, where

$$F = \left(\frac{h}{s}\right)\left(\frac{r}{r+l}\right) = 0.665$$

Thus the total incident beam is given by

$$I_0 = \frac{I_\theta}{F} = 110{,}000 \text{ counts/min}$$

where I_θ is the peak counting rate obtained from the beam profile, which we took as $I_\theta = 74{,}000$ counts/min. The above value of I_0 is subject to at least a ± 20 percent error in view of the approximations used and the nonuniformities in beam density and direction.

(c) Finally, the beam profile gives information on the true position of the beam axis. From Fig. 6.5a we find that the axis is located at $\theta_0 = -0.^{\circ}25$, and all the scattering angles must be corrected accordingly.

Now data may be taken. The chamber is opened, the scattering foil inserted, and the chamber again evacuated. The counting rate is measured as a function of angle first to the one side and then to the other side of the beam. These raw data are given in column 2 of Table 6.2. Column 3 gives the counts after background subtraction and column 4 the probable error; in column 5 are shown the corrected angles. At each angle enough data are accumulated so that the statistical accuracy is of the order of 3 percent.

In evaluating columns 3 and 4, the background rate R' was taken as 130 ± 10 counts/min (see Fig. 6.5b). The large error on the background is not due to a statistical uncertainty (which could be reduced) but to fluctuations in R' over the period that the experiment was in progress. As R becomes comparable to R', the error in the true rate $R_t = R - R'$ increases, reaching $\Delta R_t/R_t \approx 0.5$, which sets a limit to the largest useful scattering angle.

From the observed yields of scattered particles, we can obtain the differential cross section, from the expression

$$\frac{d\sigma}{d\Omega} = \frac{I_s}{(\Delta\Omega) I_0 N}$$

where the symbols are defined as on page 239 and have the same values

I_0 = 110,000 counts/min
N = 1.48×10^{19} gold nuclei/cm² (for the given thickness of the foil $t = 0.00025$ cm)
$\Delta\Omega$ = 0.02 sr (but see next paragraph)
I_s = value given by column 3 of Table 6.2

The differential cross section so obtained is shown in column 6 of Table 6.2 and is also plotted against the scattering angle in Fig. 6.7a.

The process of dividing the yield by $\Delta\Omega$ to obtain the cross section needs some further discussion. Two points are of special importance:

(a) In evaluating $\Delta\Omega$ we use the approximation

$$\Delta\Omega = \frac{hw}{l^2} = \frac{1.555 \times 0.565}{(6.66)^2} = 0.0197 \text{ sr} \qquad (2.21)$$

where w and h are the width and height of the rectangular detector and l the distance from the target (see also Fig. 6.6). The approximation is valid because the detector area is always normal to the scattered beam, and

TABLE 6.2
RUTHERFORD SCATTERING DATA

θ_{lab} (1)	R (counts/min) (2)	$R - R'$ (3)	$\Delta(R - R')$ (4)	$\theta_{correct}$ (5)	$d\sigma/d\Omega$ (observed) (6)	$(\sin^4\theta/2)^{-1}$ (7)	k (8)
					$\times 10^{-31}$ cm^2/sr	$\times 10^3$	$\times 10^{-34}$ cm^2/sr
−70°	144.3						
−60°	147.2						
−50°	139.8						
−40°	148.6						
−35°	145.2						
−30°	144.2						
−25°	166.6	37	±15	24°45′	1.13	0.460	2.46
−20°	228.6	99	±15	19°45′	3.04	1.16	2.62
−15°	443	313	±17	14°45′	9.60	3.72	2.59
−10°	1868	1738	±40	9°45′	53.4	19.2	2.78
−8°	5336	5206	±72	7°45′	160	47.9	3.34
0°	41662						
+6°	8576	8146	±90	6°15′	250	115	2.17
+8°	3663	3533	±60	8°15′	107	37.5	2.85
+10°	1681	1551	±40	10°15′	47.6	15.7	3.04
+15°	380	250	±17	15°15′	7.68	3.24	2.37
+20°	215.7	86	±15	20°15′	2.54	1.05	2.42
+25°	182.2	52	±15	25°15′	1.60	0.437	3.66
+30°	161.6	32	±15	30°15′	0.98	0.190	
+35°	163.2						
+40°	132.7						
+50°	142.1						

it becomes better as l increases, and the beam spot on the target decreases. More accurately, we must integrate the element of solid angle

$$d\Omega = \sin\theta\, d\theta\, d\varphi$$

over the area of the detector. Clearly, if we approximate and assume θ to be constant, $d\theta = \Delta\theta = w/l$, and $d\varphi = \Delta\varphi = h/(l\sin\theta)$, we obtain Eq. 2.21, which is independent of θ.

(b) In dividing the yield by $\Delta\Omega$ to obtain the differential cross section we must assume that $d\sigma/d\Omega$ does not change appreciably over the angular range subtended by the detector. This assumption is not very good, especially at the smaller scattering angles. Correctly, we should integrate $d\sigma/d\Omega$ over $d\Omega$ to obtain the yield

$$I = \int_{\varphi_1}^{\varphi_2} d\phi \int_{\theta_1}^{\theta_2} \frac{1}{\sin^4\theta/2}\sin\theta\, d\theta = \frac{4}{2}(\varphi_1 - \varphi_2)\left.\frac{1}{\sin^2\theta/2}\right]_{\theta_1}^{\theta_2}$$

but we may set $\varphi_1 - \varphi_2 \simeq h/(l\sin\bar{\theta})$ as before, and

$$I = \frac{h}{l\sin\bar{\theta}}\left[\frac{\sin^2(\theta_1/2) - \sin^2(\theta_2/2)}{\sin^2(\theta_1/2)\sin^2(\theta_2/2)}\right]$$

which approximates but is not equal to the result obtained by using Eq. 2.21

$$I = \frac{hw}{l^2}\frac{1}{\sin^4\bar{\theta}/2}$$

In order to compare the results with the theoretical prediction of the Rutherford cross section (Eq. 2.17) we give in column 7 of Table 6.2 the factor $(1/\sin^4\theta/2)$ evaluated at the appropriate angle. The observed cross section should be proportional to this factor, and column 8 gives the ratio k = (column 6)/(column 7), which should be equal to

$$k = \left(\frac{zZe^2}{4\pi\epsilon_0}\frac{1}{4E}\right)^2 \qquad (2.22)$$

In Fig. 6.7b is a log-log plot† of yield against $1/(\sin^4\theta/2)$; horizontal error bars correspond to ±0°25 uncertainty in the scattering angle,‡ while the vertical ones correspond to the errors given in column 4 of Table 6.2. Angles to the right of the beam axis are indicated by a cross, to the left of the axis by a circle.

† On a linear scale, the plot should yield a straight line of slope k. However, on the log-log plot we cover a much larger range of values; the slope of the line must be 1 and the intercept gives k.

‡ Remember, however, that the detector angular width is ±2°5.

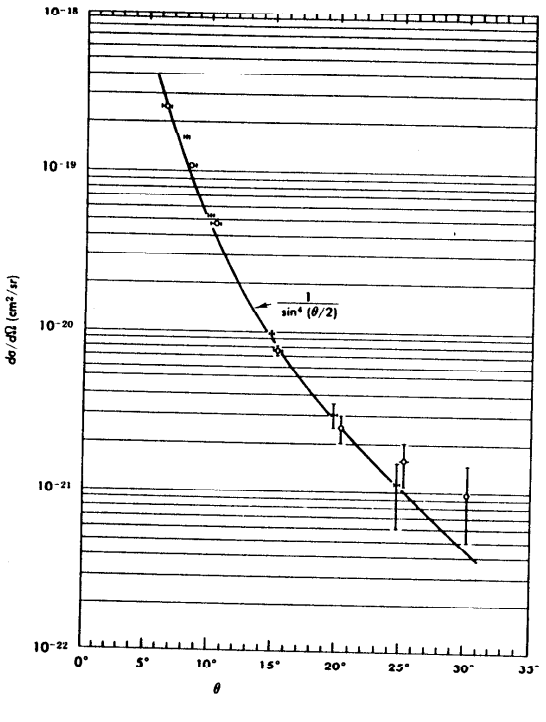

FIG. 6.7 Results of the Rutherford scattering experiment. (a) Cross section against angle; note that the measurement is extended over three decades. (b) Cross section against $1/(\sin^4\theta/2)$; note the straight line fit and the unit slope of the line.

The straight line on Fig. 6.7b is the theoretical prediction that has slope = 1.00. We note that it provides a very good fit to the experimental points over more than two decades, and therefore these data confirm the

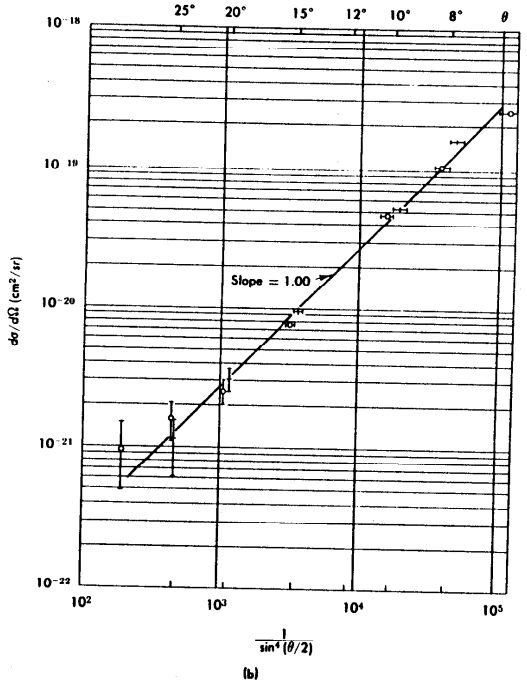

hypothesis of the nuclear atom and the angular dependence of the Rutherford scattering cross section as obtained in Eq. 2.17. The small deviations from the fit are due to experimental difficulties which will be discussed below.

While the straight line in Fig. 6.7b was constrained to have slope = 1.00, the intercept (that is, the normalization) was obtained by a least-squares fit to the data points. It yields a value

$$k = 2.70 \times 10^{-24}\ \text{cm}^2$$

Evaluation of Eq. 2.22 with $E = 5.2$ MeV yields $k = 1.20 \times 10^{-24}$ cm². However, the alpha particle loses a considerable amount of energy when traversing the target; it is therefore more appropriate to average $1/E^2$ over this energy range, that is,

$$\left\langle \frac{1}{E^2} \right\rangle = \frac{\int_{x_1}^{x_2} E^{-2}\, dx}{\int_{x_1}^{x_2} dx}$$

We assume for simplicity that the energy loss is proportional to the thickness

$$E = E_0 - \left(\frac{dE}{dx}\right)x$$

hence

$$dE = -\left(\frac{dE}{dx}\right)dx$$

and we can write

$$\left\langle \frac{1}{E^2} \right\rangle = \frac{\int_{E_1}^{E_2} E^{-2}\, dE}{\int_{E_1}^{E_2} dE} = \frac{1/E_1 - 1/E_2}{E_2 - E_1} = \frac{1}{E_1 E_2}$$

We now use $E_1 = 5.2$ MeV, $E_2 = 3.7$ MeV, and obtain from Eq. 2.22

$$k = 1.67 \times 10^{-24} \text{ cm}^2 \text{ (theory)}$$

whereas

$$k = 2.70 \times 10^{-24} \text{ cm}^2 \text{ (experiment)}$$

The difference between the observed and theoretical constants, while at first sight large, can be traced to the limited sensitivity of the apparatus and mainly to

(a) Uncertainty in incoming flux
(b) Uncertainty in foil thickness

and to a lesser extent to

(c) Extended size of the beam and lack of parallelism
(d) Extended angular size of the detector
(e) Plural scattering in the foil (for the data at small angles)
(f) Background (for the data at large angles)

The reader should keep in mind that the main purpose of the experiment was to prove the $1/(\sin^4 \theta/2)$ dependence. Further, the observed value of k is of the correct order of magnitude and if we used it to find the charge of the gold nucleus, we would obtain

$$Z' = 99 \qquad \text{instead of} \qquad Z = 79$$

It is interesting to note that when the foil was inserted, the counting rate at 0° dropped from $I_0 = 74{,}000$ to $I_0' = 41{,}660$ counts/min (see Table 6.2). This reduction is a measure of the total cross section, or more precisely of

$$I_0 - I_0' = \sigma_t N I_0 = N I_0 \int_{\theta_0}^{\pi} \frac{d\sigma}{d\Omega}(\theta)\, d\Omega$$

where for θ_0 we use the angular limits of the detector.† Then we obtain for the probability of interaction (see Eq. 2.19)

$$\frac{I_0 - I_0'}{I_0} = Nk \frac{2\pi}{\sin^2 \theta_0/2}$$

With $\theta_0 = 2°5$, $N = 1.48 \times 10^{19}$, and the observed value of

$$\frac{I_0 - I_0'}{I_0} = 0.44$$

we obtain

$$k = 2.26 \times 10^{-24} \text{ cm}^2$$

which is of the correct order of magnitude. However, in view of the crude approximations made in evaluating the total cross section, the agreement with the previously discussed values of k is fortuitous.

The large value for $(I_0 - I_0')/I_0$ indicates that the probability for scatters $\geq 2°5$ is considerable, and that therefore it is probable that an alpha particle may suffer in traversing the foil more than one (small angle) scattering from a nucleus.

We conclude this section with two further remarks:

(a) If we changed the scattering material, the cross section would also change, as $(Z/Z')^2$, while maintaining the same angular dependence. We can thus obtain information on the charge of the nucleus and confirm that it is equal to the atomic number Z of the material. Convenient target materials are silver, $Z = 47$, aluminum, $Z = 13$, and others.

† This discussion is really applicable to a beam of circular cross section and to a circular detector.

(b) For angles $\theta > \pi/2$ the cross section does not vary as rapidly, and at the limit $\theta \approx \pi$ it has the value $d\sigma/d\Omega = k = 1.2 \times 10^{-24}$ cm². Precise measurements at these large angles reveal deviations from the Rutherford equation and are due to the strong interaction (nuclear interaction, see Table 6.1) between the alpha particle and the gold nucleus.

As explained in detail in the introduction to this chapter, the nuclear interaction will manifest itself only at short distances—that is, at high-momentum transfers q (Eq. 1.4), where $q = 2p \sin \theta/2$. Clearly the maximum momentum transfer in this experiment is

$$q = 2p = 2\sqrt{2Em} = 200 \text{ MeV}/c$$

The recent experiments on Coulomb scattering of electrons from protons have been extended to $q \simeq 2.2$ BeV/c.

3. Compton Scattering

3.1 Frequency Shift and Cross Section

This section deals with the scattering of electromagnetic radiation by free electrons. As mentioned in the introduction to this chapter, it is the scattering of electromagnetic radiation from various objects that makes it possible for us to "see" them. However, as the frequency of the radiation is increased beyond the visible region, the light quanta have energies comparable to, or larger than the binding energy of the electrons in atoms, and the electrons can therefore be considered as free.

In 1920 A. H. Compton investigated the scattering of monochromatic x-rays from various materials. He observed that after the scattering, the energy (frequency) of the x-rays had changed, and had always decreased. From the point of view of classical electromagnetic theory, this frequency shift cannot be explained,† since the frequency is a property of the incoming electromagnetic wave (field) and cannot be altered by the change of direction implied by the scattering. If, on the other hand, we think of the incoming radiation as being represented by a beam of photons, we need only consider the scattering of a quantum of energy $E = h\nu$ from a free electron; then, because of energy-momentum conservation, the scattered quantum has energy $E' = h\nu' < E$, in complete agreement with the experiments of Compton.

The frequency shift will depend on the angle of scattering and can be easily calculated from the kinematics. Consider an incoming photon of energy $E = h\nu$ and momentum $p = h\nu/c$ (Fig. 6.8) scattering from an electron of mass m; $\mathbf{p}$ is the momentum of the electron after scattering and

† See, for example, J. D. Jackson, *Classical Electrodynamics*, John Wiley, p. 488.

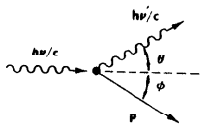

Fig. 6.8 Compton scattering of a photon from a free electron.

$h\nu'$, $\mathbf{h\nu'}/c$ the energy and momentum of the photon after the scattering. The three vectors $\mathbf{h\nu}/c$, $\mathbf{h\nu'}/c$, and $\mathbf{p}$ must lie on the same plane, and energy conservation yields

$$h\nu + mc^2 = h\nu' + \sqrt{p^2c^2 + m^2c^4} \tag{3.1}$$

From momentum conservation we obtain

$$h\nu = h\nu' \cos\theta + cp \cos\phi \tag{3.2}$$

$$0 = h\nu' \sin\theta + cp \sin\phi \tag{3.3}$$

Here θ is the photon scattering angle, and ϕ the electron recoil angle. To solve the above equations we transpose appropriately, square, and add Eq. 3.2 and Eq. 3.3 to obtain

$$h^2\nu^2 - 2h^2\nu\nu' \cos\theta + h^2\nu'^2 = c^2p^2$$

while by squaring Eq. 3.1,

$$h^2\nu^2 + h^2\nu'^2 - 2h^2\nu\nu' + 2hmc^2(\nu - \nu') = c^2p^2$$

which by subtraction yields

$$\frac{\nu - \nu'}{\nu\nu'} = \frac{h}{mc^2}(1 - \cos\theta) \tag{3.4}$$

We can recast Eq. 3.4 into two more familiar forms: (a) to give the shift in wavelength of the scattered x-ray beam:

$$\Delta\lambda = \lambda' - \lambda = \frac{h}{mc}(1 - \cos\theta) \tag{3.5}$$

or (b) to give the energy of the scattered photon:

$$E' = \frac{E}{1 + (E/mc^2)(1 - \cos\theta)} \tag{3.6}$$

From Eq. 3.5 we see that the shift in wavelength, except for the angular